Int J Adv Manuf Technol (2018) 94:1727–1744
DOI 10.1007/s00170-016-9669-y

ORIGINAL ARTICLE

Kerf taper and delamination damage minimization of FRP hybrid composites under abrasive water-jet machining

Irina Wong MM[1] · **AI Azmi**[1,2] · **CC Lee**[1] · **AF Mansor**[2]

Received: 1 August 2016 / Accepted: 27 October 2016 / Published online: 7 November 2016

Abstract Kerf taper and delamination are undesirable geometrical defects inherent to abrasive water-jet machining (AWJM) of layered fibre reinforced polymer composites. This is mainly attributed to the characteristics of water-jet energy as well as the anisotropic nature of the material. The present research describes an experimental investigation into minimizing the aforementioned defects for hybrid fibre reinforced polymer composites. Experimental results reveal that the kerf ratio was mainly influenced by the stand-off distance and traverse rate. Both sides of delamination were influenced by abrasive flow rate, traverse rate, and hydraulic pressure. Minimum kerf ratio and delamination damage can be achieved by increasing the kinetic energy of abrasive water-jet stream when impinging under a lower cutting speed. Response surface methodology (RSM) was employed for establishing empirical relationships between experimental outputs and controlled parameters. Confirmation tests have a variance of within 5% for both outputs via comparison between experimental values and the regression models.

Keywords Hybrid composites · Delamination · Kerf taper · Process modelling/statistical properties/methods · Machining

✉ AI Azmi
azwaniskandar@unimap.edu.my

[1] School of Manufacturing Engineering, Pauh Putra Campus, 02600 Pauh, Perlis, Malaysia

[2] Faculty of Engineering Technology, UniCITI Alam Campus, 02000 Pauh, Perlis, Malaysia

1 Introduction

Fundamental studies on the mechanical competence of carbon and glass fibre reinforced polymer composites have gained significant attention among research communities. The primary interest is to develop better performance composites that qualify the use of them in a broad spectrum of applications, particularly for high-performance aerospace and automotive structural components. Unfortunately, the setback of typical carbon fibre composites is that they have a low ratio of compressive-to-tensile strength, which can hinder the performance of the composites [1]. On the other hand, the glass fibre composites lack in terms of high modulus-to-weight ratio. In light of these setbacks, hybrid fibre reinforcement polymer (FRP) composites have been developed by combining two types of fibres with different configurations in a single matrix material. Hybrid composites can be classified into interply, intraply, intimately mixed hybrid and other types of mixture [2, 3]. The main idea of hybridizing the fibres is to maintain the superiority and overcome the moderate shortcomings of both fibres [1, 3, 4]. Fabrication of hybrid FRP composites usually involves preparation of fibre laminas, compaction and impregnation of the reinforcing fibres with the liquid matrix material. The steps to fabricate these composites can sometimes be time consuming and labour intensive, which lead to substantial processing costs as compared to that of injection moulding and other polymer composite processing methods. Thus, FRP composites are more or less produced to the final shape through processes such as resin infusion, pre-preg manufacturing and autoclave processes.

Despite the final or net shape processing, finishing processes that involve machining operations are still essential and are governed by a few important requirements such as meeting their intricate shape, tight dimensional and functional requirements. Trimming or machining operation is often foremost

encountered in the main operation in the manufacturing plan to bring the FRP composites to their desired and final shape prior to assembly. Therefore, the requirements of high-quality and reliable FRP composites are of ultimate importance. The reason is that there will be an increased cost of discarding the damaged piece composites. However, the heterogeneity and anisotropy of the composite materials make machining difficult and challenging. Very often, the trimming process results in many defects such as fibre pull-out, poor surface finish, fibre breaking and delamination damage that are located at the edges of the laminate [5]. Consequently, the cutting of hybrid FRP composites requires an in-depth understanding of the behaviour of different process parameters to achieve desired efficiency and accuracy. Previous understanding is that conventional machining or cutting of monolithic FRP composites involves brittle fractures with little plastic deformation. Furthermore, an adequate level of edge sharpness on the cutting tool is inevitable to shave away fibre reinforcement in the composites [6].

Conventional machining processes such as drilling and milling involve a direct contact between the cutting tool and the part to be machined. Very often, the direct contact would lead to heat generation, stress concentration, tool wear and others that would affect the surface quality. Evidence from the literature shows that the main thrust of research undertaken globally has put a significant attention on conventional machining processes of FRP composites through drilling, turning and milling [7–9]. However, only a limited number of work have considered non-conventional processes such as abrasive water-jet machining (AWJM), laser cutting and electrical discharge machining. AWJM is a kind of non-conventional process that received much attention from the manufacturing industry to trim the FRP composites compared to other machining processes. This is due to the fact that AWJM offers several advantages such as high machining versatility, minimum stresses on the FRP composites and less thermal distortion [10, 11]. Despite these advantages, the biggest challenge concerning water-jet trimming or cutting of FRP composites is to achieve and maintain the tight machining quality requirements.

Pioneering scientific studies on the AWJM for FRP composites in the late 1990s were reported by Ramulu and Arola [12, 13]. In their study, the influences of cutting parameters on the surface roughness and kerf taper of an abrasive water-jet-machined graphite/epoxy laminate have been investigated using the Taguchi experimental design. Later, Azmir and Ahsan [14] investigated the roughness of the glass fibre reinforced plastic (GFRP) composite laminate surface after abrasive water-jet cutting. They found that inclination of the hydraulic pressure has increased the kinetic energy of the abrasive particles and hence improved the capability for material removal. In addition, hydraulic pressure is considered to be the most significant factor compared to others to influence the surface roughness of the GFRP composites. Extending from the same work, Azmir and Ahsan [15] claimed that the type of abrasive materials was another factor that can be considered to be an influencing factor towards kerf ratio. In their work, a comparison between aluminium oxide and garnet abrasives was made in cutting GFRP composites. Due to the hardness of aluminium oxide, this abrasive is preferable for the AWJM process.

Shanmugam and Masood [16] recommended that high water pressure, low traverse speed and low stand-off distance should be used to minimize the kerf taper angle of graphite and glass fibre epoxy composites. In their work, a semi-analytical model was derived based on an energy conservation approach to predict the kerf ratio. Despite their claim of a highly applicable model through verification with experimental results, it was reported that the traverse speed can only be minimized within some allowable tolerance limits and cannot be completely eliminated. Added to that, Shanmugam et al. [17] reported an experimental and analytical study on delamination damage in AWJM of graphite epoxy composite. The authors asserted that delamination is initiated by the shock wave impact of the water-jet in the initial cutting stage when it targeted to the material surface [17]. The conclusion can be made from their study is that an increase in jet traverse speed will increase the maximum crack length, and in contrast, an increase in the jet pressure will decrease the maximum crack length [17].

Table 1 Mechanical strength of the hybrid FRP composites

	$[CWW]_6$			
Batch	Ultimate tensile strength	Ultimate tensile modulus	Ultimate flexural strength	Ultimate flexural modulus
	(MPa)	(GPa)	(MPa)	(GPa)
1	449.89	19.26	437.27	34.62
2	394.16	20.51	449.86	35.67
3	479.81	20.86	473.89	34.63
4	486.21	22.38	468.01	35.54
5	456.97	21.74	453.90	33.80
Mean	453.41 (±32.6)	20.95 (±1.1)	456.59 (±13.1)	34.85 (±0.7)

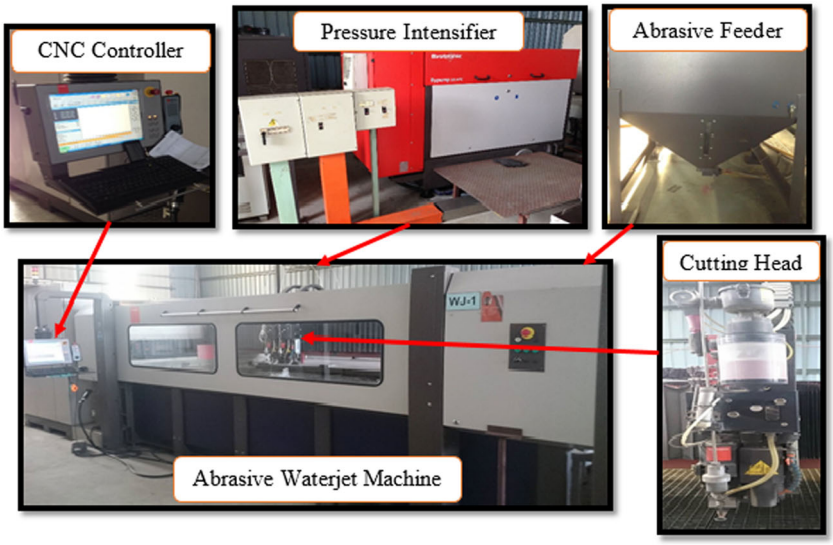

Fig. 1 Bystronic computer numerical control (CNC) water-jet cutting machine

A recent study by Alberdi et al. [11] reported the behaviour of the machinability model of carbon fibre reinforced polymer (CFRP) composites in AWJM. The machinability indices for two of the CFRP composites were found experimentally based on a previous model developed by Zeng et al. [18]. Alberdi et al. [11] claimed that the CFRP composites can be cut significantly faster than metals in AWJM. This was due to the fact that the composite materials have a significantly higher machinability index than metals (e.g. Aluminium 2024 has a machinability index of 215.3, and stainless steel 316 82.5).

It is clear that based on these reviews, there are a number of parameters that have been identified to be the most desired factor that influences the performance of AWJM for FRP composites, but only a limited amount of work on optimization of the parameter setting using the appropriate design of experiment (DOE). Apart from that, studies regarding machining of these composites through abrasive water-jet cutting are limited to plain GFRP and CFRP, where G and C represent glass and carbon respectively. Database for effective cutting of hybrid FRP composites made from carbon and glass fibres is still insufficient in the current literature. Hybrid composites have combinations of properties of the plain carbon and glass fibre that make the mechanisms of cutting of these composites even more complex and challenging.

2 Materials and experimental procedure

In the present research, carbon and E-glass woven fabrics (T300, 3K tow, 200 g/m^2) were used as reinforcement, and epoxy resin was used as matrix to fabricate interply hybrid FRP composites. In this type of hybrid FRP composites, the carbon fibre contributes the high stiffness and low density while the glass fibre enhances the failure strain and reduces the overall material cost of the composites. The hybrid FRP composites were fabricated using the vacuum-assisted resin transfer moulding process which is capable of producing high-volume fractions as well as constant and consistent thickness of composite panels compared to the hand lay-up method. Table 1 shows the mechanical properties of $[CW_2]_6$ hybrid composite arrangement which is presented in this project, where C and W are weaved carbon fibres and glass fibres, respectively. A detailed study on mechanical properties of this hybrid composite can be found in the previously reported article [19, 20].

A three-axis Bystronic computer numerical control (CNC) water-jet cutting machine available at the KTechno Sdn. Bhd. was used for experimentation (Fig. 1). The AWJ cutting machine is equipped with Bypump 50 APC ultra-high capacity pump. The pump is designed to provide a pressure of 5300 bar and driven by a dual cylinder intensifier design. The

Table 2 Details of the constant parameters in this AWJM process

Abrasive material/size	Garnet no. 80
Orifice material/diameter	Sapphire/0.28 mm
Mixing tube diameter/length	0.762 mm/69.85 mm
Nozzle material/diameter	Carbide/0.08 mm
Jet impact angle	90°

Table 3 Process parameters and their levels

Process parameters	Symbol	Units	Factor level		
			−1	0	1
Abrasive flow rate	A	g/min	120	360	600
Hydraulic pressure	B	bar	2000	2600	3200
Stand-off distance	C	mm	2	6	8
Traverse rate	D	mm/min	1000	1750	2500

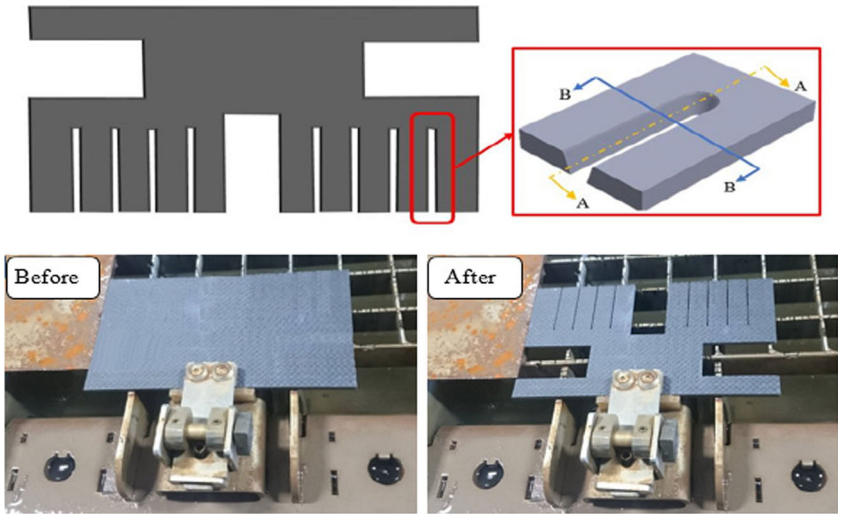

Fig. 2 Specimen design (*red box*, kerf slot) (color figure online)

sapphire orifice and the carbide mixing tube were kept constant at 0.28 and 0.76 mm in diameter, respectively. Other parameters which are kept constant are provided in Table 2. All the experimentations were carried out using Australian GMA Garnet no. 80 abrasive material. Besides that, the nozzle was frequently checked and changed with a new one once the nozzle was worn out. It is important to highlight that all machining procedures were executed using a single pass cutting.

A face-centred composite design (FCD) with a total of 30 experimental runs (16 factorial points—2^4, 8 axial points—2 × 4, and 6 centre points) has been selected and carried out using Design-Expert V8.0.6 software. Four principle machining parameters, which include abrasive flow rate, hydraulic pressure, stand-off distance and traverse rate, have been employed to investigate the influence of these parameters on the kerf ratio and delamination damage. These selected parameters have been varied in three different levels (−1, 0 and 1) and listed in Table 3, in which −1, 0 and 1 represent the minimum, centre and maximum values. The selection of a range of parameters was based on a previously reported study of AWJ cutting parameters of CFRP and GFRP as well as industrial recommendations of our research partner, KTechno Sdn. Bhd.

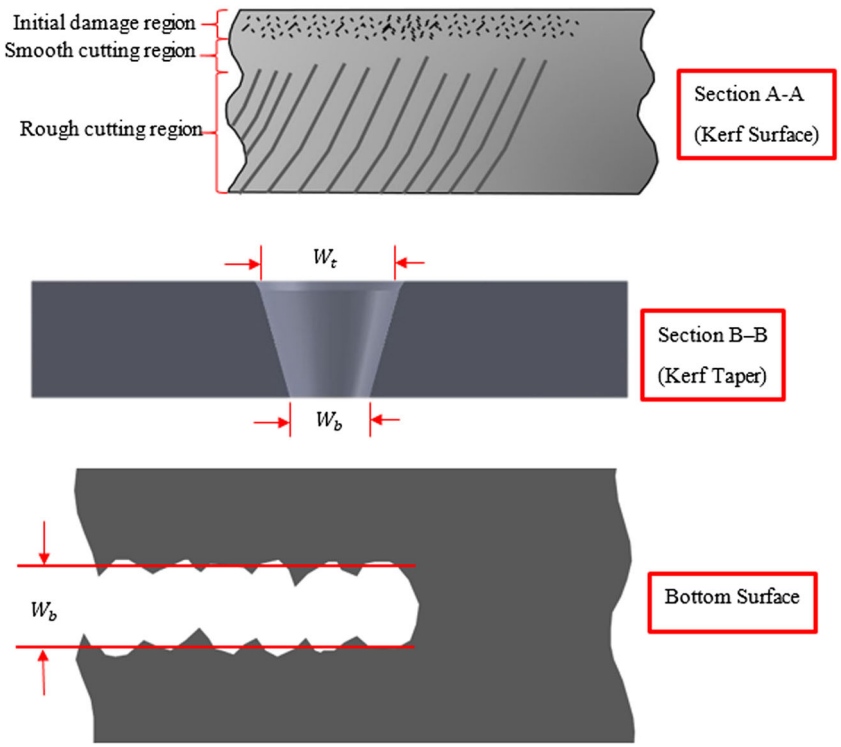

Fig. 3 Kerf geometry of a through cut composite trimmed by abrasive water-jet cutting [47]

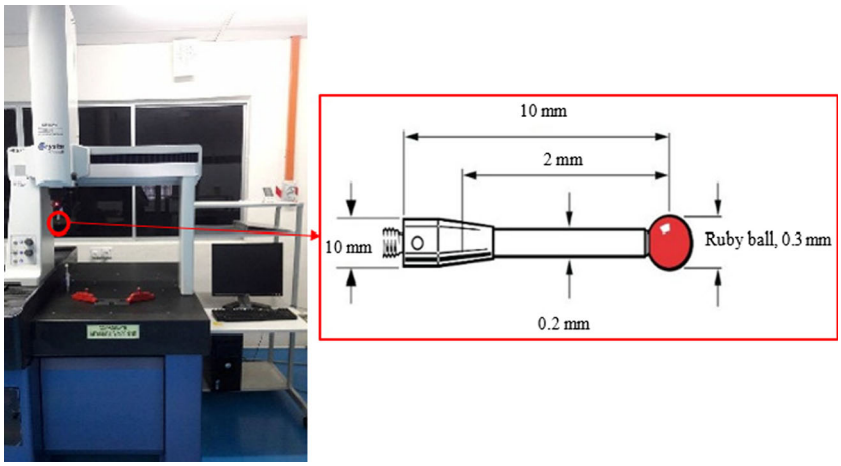

Fig. 4 Coordinate measuring machine (Mitutoyo Crysta-Plus M574) equipped with ruby ball stylus (Renishaw A-5000-7800)

Kerf ratio is defined as the proportion of top kerf width to bottom kerf width, as shown in Eq. (1). A schematic of the kerf geometry of a through cut composite trimmed by abrasive water-jet cutting is illustrated in Figs. 2 and 3. It is characterized by kerf surface topography regarding roughness, taper and waviness. The kerf ratio is one of the important outcomes of abrasive water-jet cutting because it will affect the process capability to achieving the product quality requirement.

$$\text{Kerf ratio}, T_R = \frac{W_t}{W_b} \tag{1}$$

where W_t is the top width of kerf and W_b is the bottom width of kerf.

The upper and lower kerf widths of the hybrid FRP specimen were measured using a coordinate measuring machine, Mitutoyo Crysta-Plus M574, equipped with ruby ball stylus, Renishaw A-5000-7800, as depicted in Fig. 4. At least five readings were taken on every slot of through cutting to minimize variable, and average reading was calculated.

A delamination factor (F_d) is used to determine the peel-up and push-out delamination along the slot of through cut. It was measured using a zoom lens microscope (Topper XDC-10) equipped with a VGA high-resolution camera and ImageJ software. The delamination factor (F_d) was then determined using the following equation.

$$F_d = \frac{W_{\max}}{W} \tag{2}$$

in which F_d is the factor of delamination, $W_{\max}$ is the maximum width of the delamination area and W is the actual width of cut. Readings of five trials of delamination factors for every 40-mm slot of the cutting condition were taken based on the schematic of the delamination damage shown in Fig. 5.

Table 4 Experimental results for kerf ratio based on 2^4 orthogonal array

Std	Run	Factors				Response		
		A	B	C	D	W_t (mm)	W_b (mm)	T_R
12	1	600	3200	2	2500	1.0056	0.6941	1.4489
8	2	600	3200	8	1000	1.6333	1.1299	1.4455
3	3	120	3200	2	1000	0.9916	0.7258	1.3662
9	4	120	2000	2	2500	0.9367	0.5776	1.6218
18	5	360	2600	5	1750	1.2440	0.7557	1.6462
5	6	120	2000	8	1000	1.3354	0.8191	1.6303
2	7	600	2000	2	1000	1.0151	0.7808	1.3000
14	8	600	2000	8	2500	1.6573	0.8669	1.9116
15	9	120	3200	8	2500	1.3150	0.7051	1.8650
17	10	360	2600	5	1750	1.4387	0.8324	1.7283
16	11	600	3200	8	2500	1.5618	0.8900	1.7549
19	12	360	2600	5	1750	1.3805	0.8082	1.7080
13	13	120	2000	8	2500	1.1045	0.6510	1.6967
10	14	600	2000	2	2500	0.9865	0.7198	1.3704
1	15	120	2000	2	1000	0.9291	0.6854	1.3556
4	16	600	3200	2	1000	1.0525	0.8000	1.3156
6	17	600	2000	8	1000	1.7719	1.0221	1.7336
11	18	120	3200	2	2500	0.9119	0.6602	1.3812
20	19	360	2600	5	1750	1.2399	0.7663	1.6180
7	20	120	3200	8	1000	1.3934	0.8193	1.7008

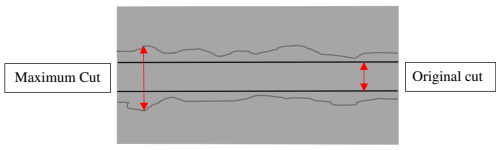

Fig. 5 Delamination damage measurement

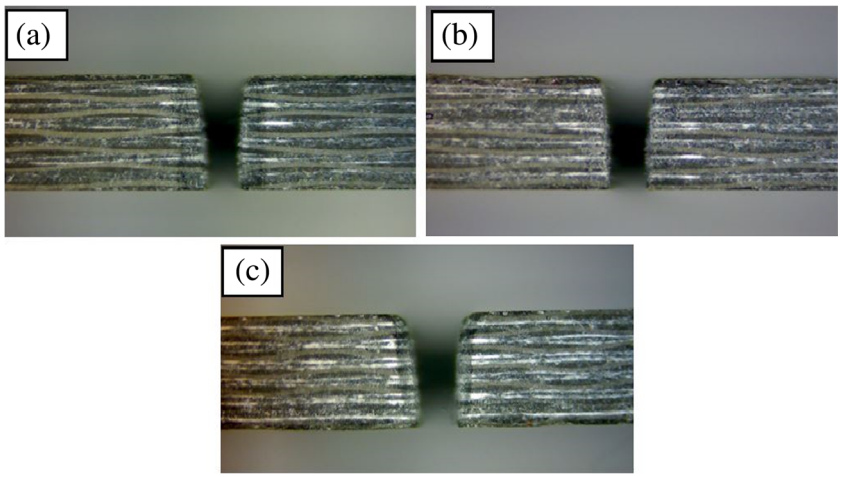

Fig. 6 Cross section of hybrid carbon/glass composites with abrasive water-jet cutting: **a** Ex. 1 (with 2 mm stand-off distance), **b** Ex. 5 (with 5 mm stand-off distance) and **c** Ex. 2 (with 8 mm stand-off distance)

3 Results and discussion

3.1 Experimental results of kerf widths and kerf ratio

To evaluate the degree of the kerf widths and ratio after trimming by AWJM, the composite specimens were cut with a full penetration over a length of 45 mm line. In each sample, the kerf widths on the top and bottom surfaces were measured at five equidistant points along the length of the cut using a coordinated measuring machine. The top kerf width, bottom kerf width, kerf ratio and T_R values were averaged for each of the experimental parameters and tabulated in Table 4. It

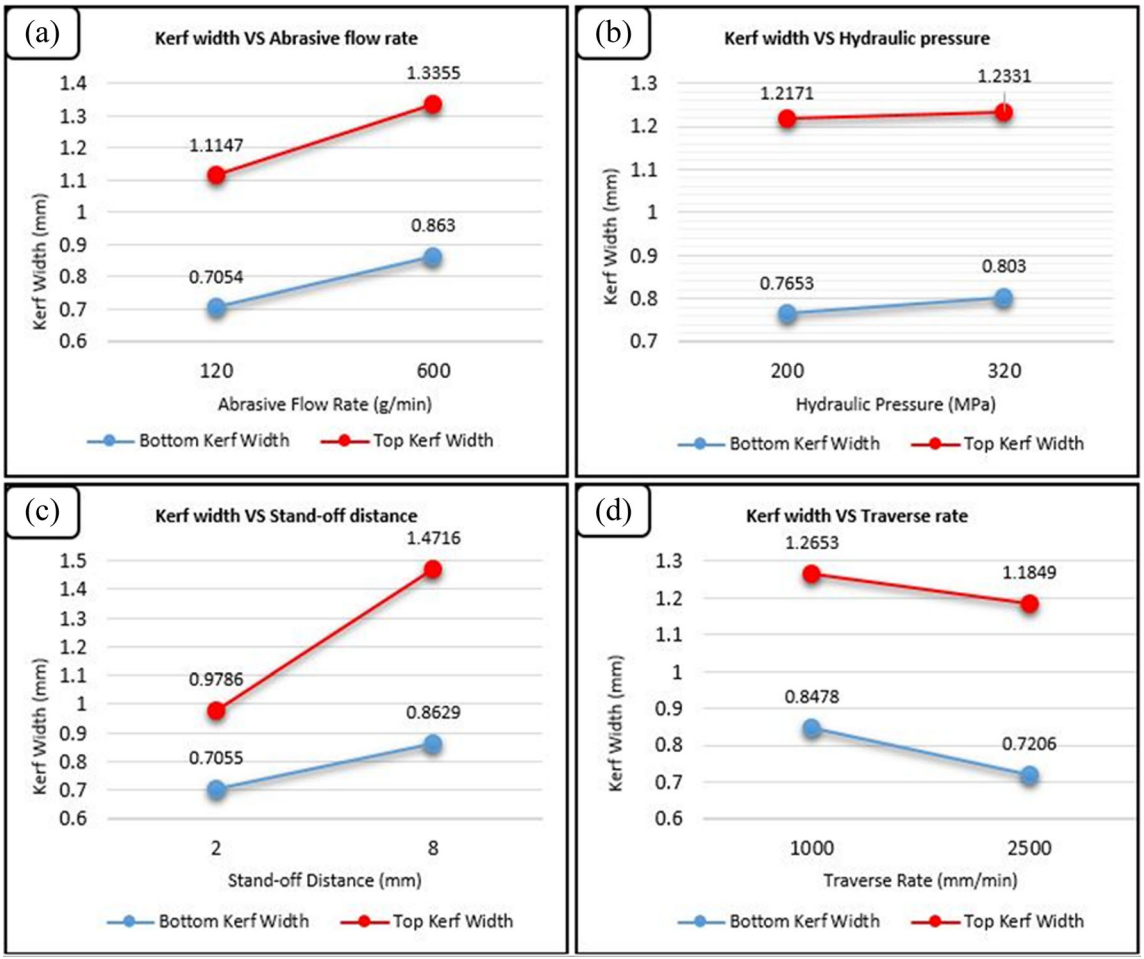

Fig. 7 Main effect *plots* of top and bottom kerf width

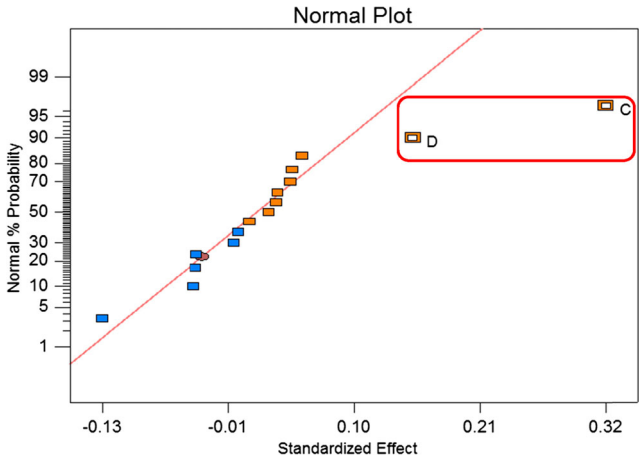

Fig. 8 Normal probability *plot* of the kerf ratio for the 2^4 factorial design

appears that the kerf ratio was in the range of 1.300 to 1.912. These results were then inputted into the Design-Expert V8.0.6 software for further statistical analyses.

The cross section of the machined hybrid FRP composites from different experimental runs are shown in Fig. 6 for various stand-off distances. From the figure shown, it is apparent that a kerf-tapered slot is created, with the top surface wider than the bottom. The representative trends and relationships between the kerf geometries (top and bottom kerf widths) together with the AWJM process parameters are shown in Fig. 7. A general observation that can be drawn from these figures is that the kerf width increases with higher abrasive flow rate, hydraulic pressure and stand-off distance, whereas it declines with an increase in traverse rate. Detailed discussions on the effects of each parameter are given as follows:

3.1.1 Effect of abrasive flow rate on kerf widths

Figure 7a depicts the influence of abrasive flow rate on both top and bottom kerf widths. The percentage contribution of abrasive concentration on the top and bottom kerf widths is 19.8 and 22.3%, respectively. The rise of abrasive quantities leads to a higher concentration of the water-jet stream. Due to this, the dense packing of abrasives increases the inter-particular collision and creates high kinetic energy of the water-jet stream to impinge on the cutting composite surface during the trimming process and thus contributes a wider kerf. It is important to note that the current result well agreed with the conclusion made by Doreswamy et al. [21].

3.1.2 Effect of hydraulic pressure on kerf widths

From Fig. 7b, it is evidenced that there is only a marginal increase in both top and bottom kerf widths with the increase in hydraulic pressure. The percentage contribution of the hydraulic pressure on the top kerf width is 1.3% and the bottom kerf width 4.9%, respectively. With a higher water pressure, a greater kinetic energy as well as flow turbulence of water-jet stream can impinge through the hybrid FRP composites to open a wider slot. Flow turbulence enhances the inter-particular collision and also the water-jet expansion, which leads to an increase in the kerf width. Doreswamy et al. have drawn the same assumption with the study on abrasive water-jet machining on graphite/glass hybrid FRP composites [21].

3.1.3 Effect of stand-off distance on kerf widths

Stand-off distance refers to the distance between the water-jet nozzle and the surface of the hybrid FRP composites. It is clearly shown that a higher stand-off distance tends to produce a wider kerf as illustrated in Fig. 7c. It is interesting to note that the stand-off distance exhibits a significant incline effect on the top kerf width when changing from 2 to 8 mm. The percentage contribution on the top and bottom kerf widths shows a 50.4 and 22.3% inclination, respectively. The kerf widths produced from different stand-off distances (2, 5 and 8 mm) can be observed in Fig. 7. As anticipated, increasing the stand-off distance between the nozzle and the workpiece will create a huge variation between top and bottom kerf widths which eventually produces a higher kerf ratio. According to Ramulu and Arola

Table 5 ANOVA table for kerf ratio

Source	Sum of squares	DF	Mean square	*F* value	*P* value Prob > *F*	
Block	0.0054	1	0.0054			
Model	0.5060	2	0.2530	29.5571	<0.0001	Significant
C—stand-off distance	0.4156	1	0.4156	48.5474	<0.0001	
D—traverse rate	0.0905	1	0.0905	10.5668	0.0054	
Curvature	0.0453	1	0.0453	5.2937	0.0362	Significant
residual	0.1284	15	0.0086			
Lack of fit	0.1210	13	0.0093	2.5083	0.3209	Not significant
Pure error	0.0074	2	0.0037			
Cor. total	0.6852	19				
Std. Dev.	0.10	R^2		0.7444		
Mean	1.58	Adj. R^2		0.7125		
C.V.%	6.60	Pred. R^2		0.6022		
PRESS	0.27	Adeq Precision		10.850		

Table 6 Augmented design of experiment for kerf ratio

Std	Run	Block	Factors				Response		
			A	B	C	D	W_t (mm)	W_b (mm)	T_R
26	21	Block 3	360	2600	8	1750	1.5309	0.9103	1.681723
21	22	Block 3	120	2600	5	1750	1.1076	0.7014	1.579023
29	23	Block 3	360	2600	5	1750	1.3840	0.8367	1.654221
22	24	Block 3	600	2600	5	1750	1.3774	0.8209	1.677992
27	25	Block 3	360	2600	5	1000	1.4103	0.9010	1.565321
25	26	Block 3	360	2600	2	1750	1.0301	0.7411	1.390039
23	27	Block 3	360	2000	5	1750	1.2208	0.8007	1.524616
28	28	Block 3	360	2600	5	2500	1.2684	0.7707	1.645674
30	29	Block 3	360	2600	5	1750	1.2349	0.7190	1.717696
24	30	Block 3	360	3200	5	1750	1.3453	0.6952	1.935068

[12, 13], the higher stand-off distance allows water-jet stream to expand together with the lower density of abrasive particles on the outer circumference of the diverging water-jet before impingement to the workpiece. Divergence jet will penetrate through the surface of fibre laminate and hence produce a wider kerf on the top surface. Later, the water-jet stream loses its momentum as well as kinetic energy. As a consequence, the outer circumference of the diverged jet does not affect much as it approaches the lower part of the kerf [22].

3.1.4 Effect of traverse rate on kerf width

From Fig. 7d, it is noticeable that the effect of traverse rate appears to be inversely proportional to the kerf widths. This phenomenon occurred since the rapid passing of the abrasives from the nozzle only allows fewer abrasive particles to penetrate the targeted hybrid fibre laminate and hence generates a narrower slot [15, 22, 23]. Due to the reduction in the exposure period, kerf width decreases significantly, especially at the bottom laminate compared with that at the top. Hence, this increases the trend of the kerf ratio.

3.1.5 Statistical analyses on the effects of experimental parameters on kerf ratio

The normal probability plot of the effect of AWJM parameters on the kerf ratio is shown in Fig. 8. All of the parameter effects that lie along the line are negligible, whereas the large effect parameters (red box) are far from that line. Those effects that are negligible are probably due to the noise in the system. The significant effects of the experimental parameters on the kerf ratio that arise from this response are the main effects of C and D, which are the stand-off distance and traverse rate, respectively. The acquired experimental results were further analysed using statistical analysis of variance (ANOVA) in order to evaluate the effect of process parameters at the 95% confidence level. The result is depicted in Table 5. These statistical evaluations implied that the models can well describe the

Table 7 ANOVA of kerf ratio quadratic model

Source	Sum of squares	DF	Mean square	*F* value	*P* value Prob > *F*	
Block	0.027226	2	0.013613			
Model	0.620097	3	0.206699	20.56788	<0.0001	Significant
C—stand-off distance	0.457705	1	0.457705	45.54462	<0.0001	
D—traverse rate	0.091505	1	0.091505	9.105305	0.0060	
C^2	0.070887	1	0.070887	7.053707	0.0138	
Residual	0.24119	24	0.01005			
Lack of fit	0.231755	21	0.011036	3.509001	0.1643	Not significant
Pure error	0.009435	3	0.003145			
Cor. total	0.888514	29				
Std. Dev.	0.100248	R^2		0.719965		
Mean	1.598995	Adj. R^2		0.684961		
C.V.%	6.269418	Pred. R^2		0.58796		
PRESS	0.354885	Adeq Precision		11.02778		

experimental data since the F value of the model is 29.55, which indicates that the model is significant. There is only a 0.01%chance that the model could occur due to noise. Furthermore, the R^2 value of 74.44% confirms adequate, reliable and accurate experimental data. The statistical results also lead to the conclusion that the process factors C and D have a significant influence on the response since the P value corresponding to each of this factor is less than 0.05 (corresponding to 95% confident level).

Meanwhile, the "curvature F value" of 5.2937 indicates that the curvature (as measured by the difference between the average of the centre points and the average of the factorial points) in the design space is significant. This implies that there is a possibility for applying the response surface methodology (RSM) for modelling the experimental relationships. The "lack-of-fit F value" of 0.32 shows that the "lack of fit" is not significant. There is a 32.09% chance that a lack-of-fit F value this large could occur due to noise. This is good since it implies that the model is fit enough. From this result, it is evidence that the stand-off distance (C) is the factor that affects the most on the kerf ratio, since it records the lowest P value which is less than 0.0001, followed by traverse rate (D). The terms that are not significant were removed through the backward eliminating procedure.

The experimental analysis continues with the empirical modelling of the kerf ratio using RSM. This methodology provides a systematic procedure for determining the relationship between independent input process parameters and the experimental responses. The significance of the curvature indicates the possibility of developing a second-order equation for optimizing the water-jet parameters to minimize the kerf ratio. Thus, an augmented design of experiment has been applied to increase the experimental runs. A face-centred central composite design (FCD) was selected by adding ten more runs (eight axial points with two centre points) of experiments to increase the range of parameter values. The augment design together with its kerf ratio, T_R, results is tabulated in Table 6. The ANOVA results for the kerf ratio of the empirical model are presented in Table 7. Empirical models were carried out at a 95% level confidence. It can be observed that the F values of regression models were greater than the theoretical Fisher value, $F_{0.05,1,29} = 4.18$. The coefficient of determination (R^2) of the empirical model was found to be 0.72. Besides that, "Adeq Precision" is a measure of the range in the predicted response relative to its associated error. In other words, it represents the signal-to-noise ratio. A ratio greater than 4 is desirable. Adeq Precision was found to be 11.03 (more than 4), which implies an adequate signal. From the acquired experimental data, the model that has been obtained in actual units for the kerf ratio can be represented as

$$T_R = 0.90221 + 0.18818\,\mathrm{C} + 9.50658 \times 10^{-5}\,\mathrm{D} - 0.013503\,\mathrm{C}^2 \quad (3)$$

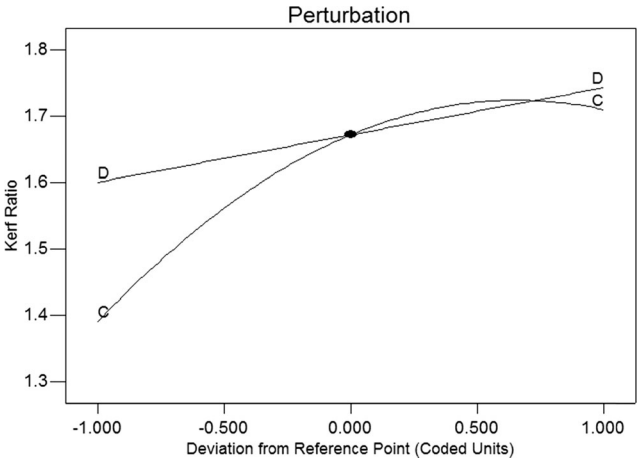

Fig. 9 *Perturbation plot* showing the effect of stand-off distance and traverse rate on T_R

3.1.6 Perturbation plot

The specific effect of each parameter on the response is another important concern in process modelling, which can be shown by a statistical measure termed as a perturbation plot. This plot facilitates the comparison on the influences of each process parameter based on the centre point of the design plot. From the perturbation plot, Fig. 9 represents the effect of the stand-off distance and traverse rate on the kerf ratio after machining. The

Table 8 Experimental results for delamination factor based on 2^4 orthogonal array

Std	Run	Factors				F_d	
		A	B	C	D	Entrance	Exit
12	1	600	3200	2	2500	2.3612	1.8702
8	2	600	3200	8	1000	2.2043	2.1650
3	3	120	3200	2	1000	2.1976	2.1000
9	4	120	2000	2	2500	3.3207	3.6005
18	5	360	2600	5	1750	2.7644	2.2478
5	6	120	2000	8	1000	2.7002	2.2240
2	7	600	2000	2	1000	1.9252	1.9123
14	8	600	2000	8	2500	2.4152	2.1922
15	9	120	3200	8	2500	2.4829	2.3330
17	10	360	2600	5	1750	2.6127	2.2384
16	11	600	3200	8	2500	2.0582	2.0706
19	12	360	2600	5	1750	2.6056	2.2877
13	13	120	2000	8	2500	2.7597	3.3748
10	14	600	2000	2	2500	2.5964	2.2158
1	15	120	2000	2	1000	2.6188	2.4715
4	16	600	3200	2	1000	1.9311	1.6989
6	17	600	2000	8	1000	2.4639	1.8156
11	18	120	3200	2	2500	2.8250	2.1671
20	19	360	2600	5	1750	2.7652	2.0782
7	20	120	3200	8	1000	2.3405	1.8982

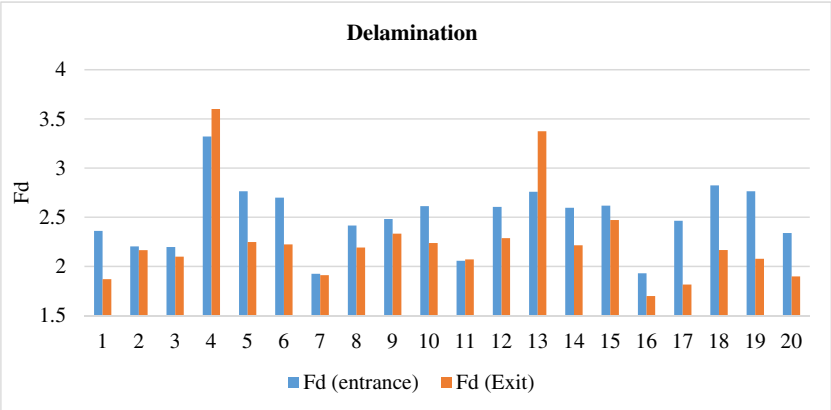

Fig. 10 A *bar chart* of delamination factor change in entrance and exit jet

perturbation plot shows a slight bending curve for the stand-off distance (C), which confirms that the kerf ratio response was principally sensitive to this factor. Comparatively, the flat traverse rate (D) line displays less sensitivity of this parameter compared with that of the stand-off distance.

3.2 Experimental results of delamination factor

For this response, the degree of delamination damage has been observed on both sides of the laminate composite, which is at the jet entrance and exit sides. The calculated delamination factor values were averaged out for each of the experimental parameters and tabulated in Table 8. The average arithmetic value of the delamination factor appears to be in between 1.931 and 3.321 for the entrance side, whereas 1.699 and 3.601 for the exit side. The bar chart, as shown in Fig. 10, compares the delamination factor for the jet entrance and jet exit sides for the 20 experimental runs. As apparent, the overall delamination damage or factor is more severe on the jet entrance side as compared to the bottom side. It has been reported by previous researchers that delamination damage on the top surface is due to the shock wave impact of the abrasive particles that reach the top surface during propagation of the water-jet [17, 24]. Nevertheless, a closer observation shows that the delamination factor on the exit side is only serious or severe for experiments 4 and 13. It is noteworthy that the parameters setting for both of these experiments are the same apart from the stand-off distance. The abrasive flow rate, hydraulic pressure and traverse rate for both of the experiments were set at 120 g/min, 200 MPa and 2500 mm/min, respectively. On the other hand, the stand-off distance for experiment 4 was 2 mm and 8 mm for experiment 13. The conclusion that can be made for this circumstance is that the combination of little abrasive flow rate, low hydraulic pressure and high traverse rate will cause a serious delamination on the bottom side.

As the abrasive particles gradually cut through the composite laminate, the reduced kinetic energy of the abrasive water-jet causes the bending fractures of the fibres and washes out the free polymer matrix in between the fibres [25]. This phenomenon causes severe delamination damage on the exit side of the water-jet. The penetration process of the abrasive jet can be depicted in Fig. 11. The overall effects of the AWJM process parameter (while keeping the other variable as constant) on the delamination factor are shown in Fig. 12. The general trend that can be drawn from this figure is that the delamination factor on the entrance side is much serious than the exit side, as stated earlier. Detailed discussions for each of the parametric effects are as follows.

3.2.1 Effect of abrasive flow rate on delamination

In the case of abrasive flow rate, the delamination factor decreases gradually with the increase in abrasive flow

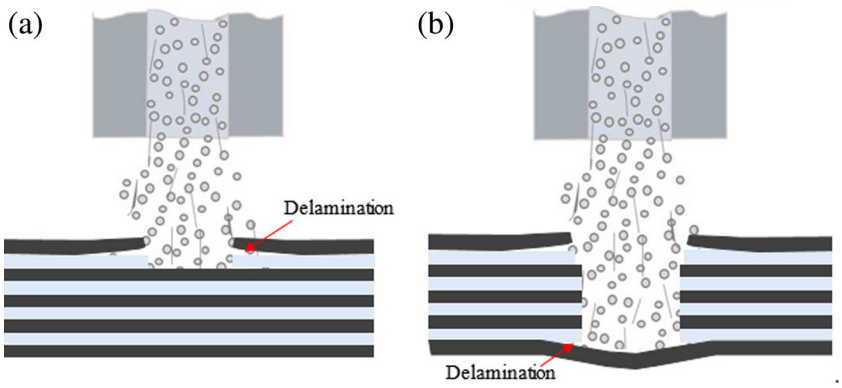

Fig. 11 Mechanism of delamination: **a** fracture initiation and **b** water-jet-induced delamination at exit

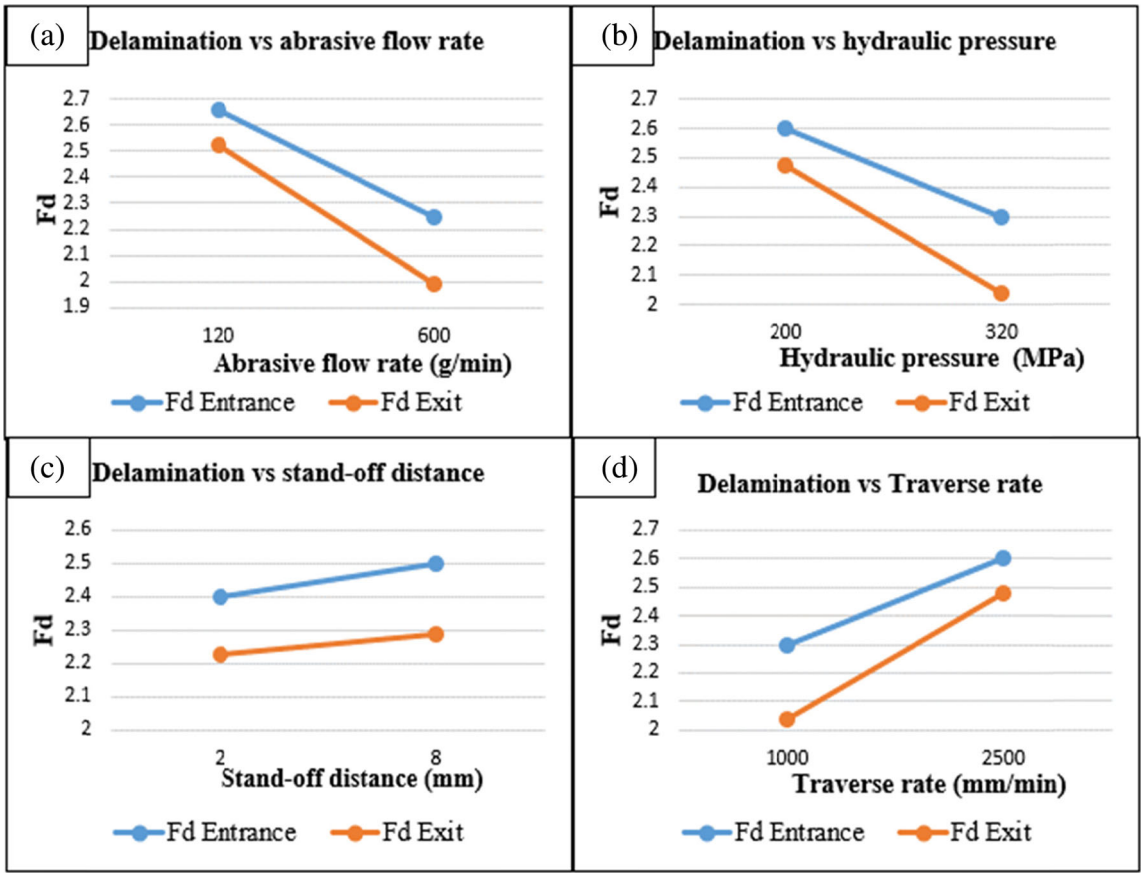

Fig. 12 Main effect *plots* of delamination on composite material

rate for both entrance and exit sides, as depicted in Fig. 12a. Abrasive flow rate determines the number of impacting abrasive particles as well as the total kinetic energy available. Therefore, a large amount of abrasive particles tends to intensify the momentum of collision to penetrate the targeted workpiece area. Consequently, the coarse-grained abrasive particles can trim and wear away the uncut fibre neatly.

3.3 Effect of hydraulic pressure on delamination factor

From Fig. 12b, the delamination factor decreases moderately on the entrance and exit sides with change in hydraulic pressure from 200 to 320 MPa. Penetration of the water-jet under high hydraulic pressure generally will arouse the fracture of laminate plies due to shock loading of the water [26]. Higher water pressure generates a larger shock wave that produces delamination damage during the piercing process. Since trimming follows the piercing process, this process might not be affected by the large shock impact generated earlier during the initiation of the piercing process. Higher hydraulic pressure tends to maintain the kinetic energy of the abrasive particles to progressively cut through the composite laminate. This cutting action produced a small degree of bending fractures of the fibre and gave a clean kerf border. Due to this fact, delamination damage alleviates with the increase in hydraulic pressure.

3.3.1 Effect of stand-off distance on delamination factor

Figure 12c shows that the delamination factor slightly decreases with the change in stand-off distance from 2 to 8 mm. As the stand-off distance increases, the water-jet diverges and increases its cutting diameter prior to penetration to the final layer of the composite laminate [24, 26]. This created

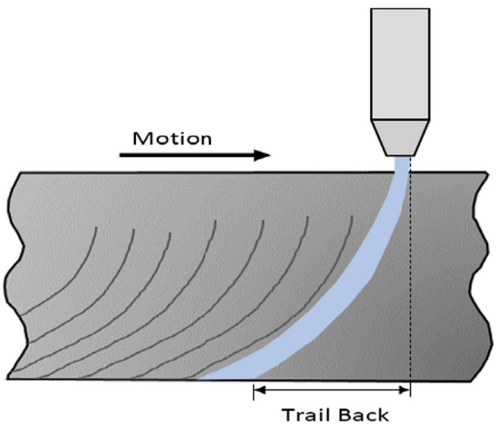

Fig. 13 Cutting front with abrasive water-jet at high traverse speeds

Table 9 ANOVA analysis for $F_{d(\text{entrance})}$ (after backward elimination, P value <0.05)

Source	Sum of squares	*df*	Mean square	*F* value	*P* value Prob > *F*	
Block	0.0000	1	0.0000			
Model	1.8457	6	0.3076	25.9736	<0.0001	Significant
A—abrasive flow rate	0.6765	1	0.6765	57.1198	<0.0001	
B—hydraulic pressure	0.3598	1	0.3598	30.3757	0.0002	
C—stand-off distance	0.0077	1	0.0077	0.6502	0.4371	
D—traverse rate	0.3714	1	0.3714	31.3593	0.0002	
AC	0.0633	1	0.0633	5.3464	0.0411	
CD	0.3670	1	0.3670	30.9904	0.0002	
Curvature	0.1796	1	0.1796	15.1649	0.0025	Significant
residual	0.1303	11	0.0118			
Lack of fit	0.1060	9	0.0118	0.9724	0.6039	Not significant
Pure error	0.0242	2	0.0121			
Cor. total	2.1556	19				
Std. Dev.	0.160697	R^2		0.856242		
Mean	2.497437	Adj. R^2		0.784363		
C.V.%	6.434489	Pred. R^2		0.664886		
PRESS	0.722371	Adeq Precision		14.23313		

a larger penetration surface. Anyhow, the stand-off distance is a less significant parameter in deciding the delamination damage of the hybrid FRP composites when compared with other parameters. This is discussed in the later section of this paper.

3.3.2 Effect of traverse rate on delamination factor

Figure 12d depicts the influence of the traverse rate on delamination damage. The trend line indicates that the delamination factor increases with higher traverse rate of the focusing nozzle. With the higher speed of the travelling nozzle across the penetrating area, it causes less number of abrasive particles to overlap cutting or machining motion. This attributed to the unclean cuts of the fibre reinforcements. Another essential explanation that has been pointed out by Abrate and Walton [27] is that the high traverse speeds cause severe delamination due to the anisotropic layered composite materials. By increasing the traverse speed, the penetration jet is bent and

Table 10 ANOVA analysis for $F_{d(\text{exit})}$ (after backward elimination with P value <0.05)

Source	Sum of squares	*df*	Mean square	*F* value	*P* value Prob > *F*	
Block	0.032401	1	0.032401			
Model	3.782535	6	0.630422	22.86164	<0.0001	Significant
A—abrasive flow rate	1.117513	1	1.117513	40.52551	<0.0001	
B—hydraulic pressure	0.767245	1	0.767245	27.82336	0.0003	
D—traverse rate	0.78265	1	0.78265	28.38202	0.0002	
AB	0.504562	1	0.504562	18.29742	0.0013	
AD	0.256213	1	0.256213	9.291314	0.0111	
BD	0.354352	1	0.354352	12.85023	0.0043	
Curvature	0.006148	1	0.006148	0.222943	0.6460	Not significant
Residual	0.303331	11	0.027576			
Lack of fit	0.281342	9	0.03126	2.843218	0.2873	Not significant
Pure error	0.021989	2	0.010995			
Cor. total	4.124415	19				
Std. Dev.	0.160592	R^2		0.92437		
Mean	2.24809	Adj. R^2		0.886555		
C.V.%	7.143502	Pred. R^2		0.741587		
PRESS	1.05743	Adeq Precision		16.77899		

Table 11 Augmented design of experiment for delamination factor

Std	Run	Block	Factors				F_d	
			A	B	C	D	Entrance	Exit
26	21	Block 3	360	2600	8	1750	1.99227	2.218714
21	22	Block 3	120	2600	5	1750	1.98521	2.224219
29	23	Block 3	360	2600	5	1750	1.96838	2.016114
22	24	Block 3	600	2600	5	1750	1.92786	1.961762
27	25	Block 3	360	2600	5	1000	1.91848	1.794397
25	26	Block 3	360	2600	2	1750	1.76412	2.225423
23	27	Block 3	360	2000	5	1750	1.97506	2.216698
28	28	Block 3	360	2600	5	2500	1.9491	2.130148
30	29	Block 3	360	2600	5	1750	1.95084	2.274752

forms a curved-cutting front (Fig. 13). This cutting front leads to a significant normal force applied to the lower layers; hence, severe delamination takes place.

3.3.3 Statistical analyses on the effects of experimental parameters on delamination factor

Experimental data were then analysed using statistical analysis of variance in identifying the significant parameter settings and relative importance of each factor to minimize delamination damage. Tables 9 and 10 displayed the summary of ANOVA outputs for the delamination factor on the entrance and exit sides, respectively. The terms that are not significant were removed through a backward elimination procedure. *F* values of each parameter at the 95% confidence level are considered as significant factors to the delamination factor when the value is higher than the statistical table value ($F_{0.05,\ 1,\ 19} = 4.38$). It is determined that the abrasive flow rate (A) is the factor which affects the most since it records the lowest *P* value of less than 0.0001. This is followed with traverse rate (D), hydraulic pressure (B) and stand-off distance (C).

Based on the ANOVA results for the delamination factor on the exit side (Table 10), it can be observed that the curvature of the graph is not sufficient enough to develop a second-order equation. This means that a two-factorial interaction equation is adequate to satisfy the requirements for an optimum condition. Therefore, an augmented design of experiment has been applied to increase the experimental runs (Table 11). Similar to that of kerf widths, FCD was selected by adding ten more runs of experiments (eight axial points with two centre points) in the existing experiments to increase the range of parameters. Results for delamination on the entrance and exit sides of the empirical models are rendered in Tables 12 and 13. Both of the regression models were carried out at a level confidence of 95%. The results implied that the experimental trend can be described by these models. This conclusion was made based on the Fisher values from the ANOVA table. The results also implied that there is only a 0.01%chance that a "model *F* value" could occur due to noise. Furthermore, the R^2 of each regression model was found to be 0.83 and 0.89 for F_d (entrance) and F_d (exit), respectively. It is clear that the value for R^2 is adequately close to 1, which indicates that the experimental data can represent the model very well.

The conclusion that can be made from Table 12 is that the process parameters A, B, C, D, CD and C^2 played a significant influence on the delamination damage or factor. This is shown

Table 12 ANOVA of $F_{d(\text{entrance})}$ quadratic model

Source	Sum of squares	*df*	Mean square	*F* value	*P* value Prob > *F*	
Block	2.0970	2	1.0485			
Model	1.8190	6	0.3032	16.9729	<0.0001	Significant
A—abrasive flow rate	0.6225	1	0.6225	34.8505	<0.0001	
B—hydraulic pressure	0.3307	1	0.3307	18.5124	0.0003	
C—stand-off distance	0.0008	1	0.0008	0.0470	0.8305	
D—traverse rate	0.3385	1	0.3385	18.9505	0.0003	
CD	0.3670	1	0.3670	20.5491	0.0002	
C^2	0.1595	1	0.1595	8.9281	0.0070	
Residual	0.3751	21	0.0179			
Lack of fit	0.3507	18	0.0195	2.3968	0.2572	Not significant
Pure error	0.0244	3	0.0081			
Cor. total	4.2911	29				
Std. Dev.	0.133647	R^2		0.829043		
Mean	2.310488	Adj. R^2		0.780198		
C.V.%	5.784347	Pred. R^2		0.630343		
PRESS	0.811048	Adeq Precision		17.69007		

Table 13 ANOVA of $F_{d(\text{exit})}$ two-interaction model

Source	Sum of squares	*df*	Mean square	*F* value	*P* value Prob > *F*	
Block	0.1574	2	0.0787			
Model	3.8750	6	0.6458	27.7917	<0.0001	Significant
A—abrasive flow rate	1.1205	1	1.1205	48.2188	<0.0001	
B—hydraulic pressure	0.8053	1	0.8053	34.6544	<0.0001	
D—traverse rate	0.8341	1	0.8341	35.8918	<0.0001	
AB	0.5046	1	0.5046	21.7127	0.0001	
AD	0.2562	1	0.2562	11.0249	0.0033	
BD	0.3543	1	0.3543	15.2475	0.0008	
residual	0.4880	21	0.0232			
Lack of fit	0.4326	18	0.0240	1.3008	0.4736	Not significant
Pure error	0.0554	3	0.0185			
Cor. total	4.5203	29				
Std. Dev.	0.152441	R^2		0.888149		
Mean	2.197899	Adj. R^2		0.856192		
C.V.%	6.935755	Pred. R^2		0.70665		
PRESS	1.279878	Adeq Precision		19.37451		

by the *P* value corresponding to each of the variables, which is less than 0.05 (corresponding to 95% confidence level) except for the stand-off distance (C). However, the stand-off distance has to be considered in the statistical analyses because it shows a significant influence while interacting with other variables. It is worthwhile to note that the parameters A, B, C and D represent the abrasive flow rate, hydraulic pressure, stand-off distance and traverse rate, respectively. The final equations of delamination in terms of the coded factor are given below:

$$F_{d\ (\text{entrance})} = 1.88221 - 7.74845 \times 10^{-4}\,\text{A} - 2.25893 \times 10^{-4}\,\text{B} + 0.31805\,\text{C} + 5.19415 \times 10^{-4}\,\text{D} - 6.7315 \times 10^{-5}\,\text{CD} - 0.020252\,\text{C}^2 \quad (4)$$

$$F_{d\ (\text{exit})} = 2.19318 - 3.01567 \times 10^{-3}\,\text{A} - 2.17765 \times 10^{-4}\,\text{B} + 1.3999 \times 10^{-3}\,\text{D} + 1.23321 \times 10^{-6}\,\text{AB} - 7.03 \times 10^{-7}\,\text{AD} - 3.30695 \times 10^{-7}\,\text{BD} \quad (5)$$

3.3.4 Effect of interaction parameters on delamination

The variations of delamination factor were further analysed by generating 3D response surface plots, Figs. 14 and 15, respectively. This surface plots represent the interaction effect between the variables or parameters, which were identified earlier. The influence of varying the two variables, stand-off distance (C) and traverse rate (D), on delamination damage of the trimmed hybrid composite laminate decreased on the entrance side. This was found when the abrasive flow rate and hydraulic pressure are kept constant at 360 g/min and 260 MPa, respectively. From Fig. 14, it is observed that the decrease in the traverse rate of the focusing nozzle combined with the lower stand-off distance can generate low delamination damage at the entrance side. This could be attributed to the perpendicular penetration (without bending) of the water-jet on the composite laminate. Hence, the curved-cutting front as discussed earlier is not created. This reduces the water-jet divergence and increases the kinetic energy of the abrasive particle to penetrate through the composite laminate. In summary, by combining small traverse rate and stand-off distance between the nozzle and the workpiece, the high momentum of the abrasive particle allows

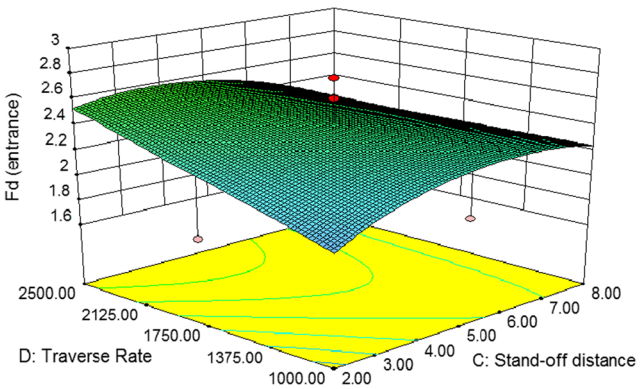

Fig. 14 Response surface and contour plots on interaction on $F_{d(\text{entrance})}$ (abrasive flow rate = 360 g/min and hydraulic pressure = 2600 mm/min)

overlapping of machining motion. This attributed to neatly shaving of the fibre reinforcement in the composite. It is evident from Fig. 15a that a finer delamination on the exit side can be achieved at the highest abrasive flow rate combined with the highest hydraulic pressure. Highest traverse speed coupled with the lowest amount of abrasive flow rate also leads to acceptable delamination damage. However, Fig. 15c reveals that the delamination damage tends to deteriorate with the growth of traverse rate and decrease in hydraulic pressure. Therefore, the conclusion that could be drawn here is that the minimum delamination on the exit side can be achieved by increasing the kinetic energy of the penetrated water-jet when impinging to the composite workpiece.

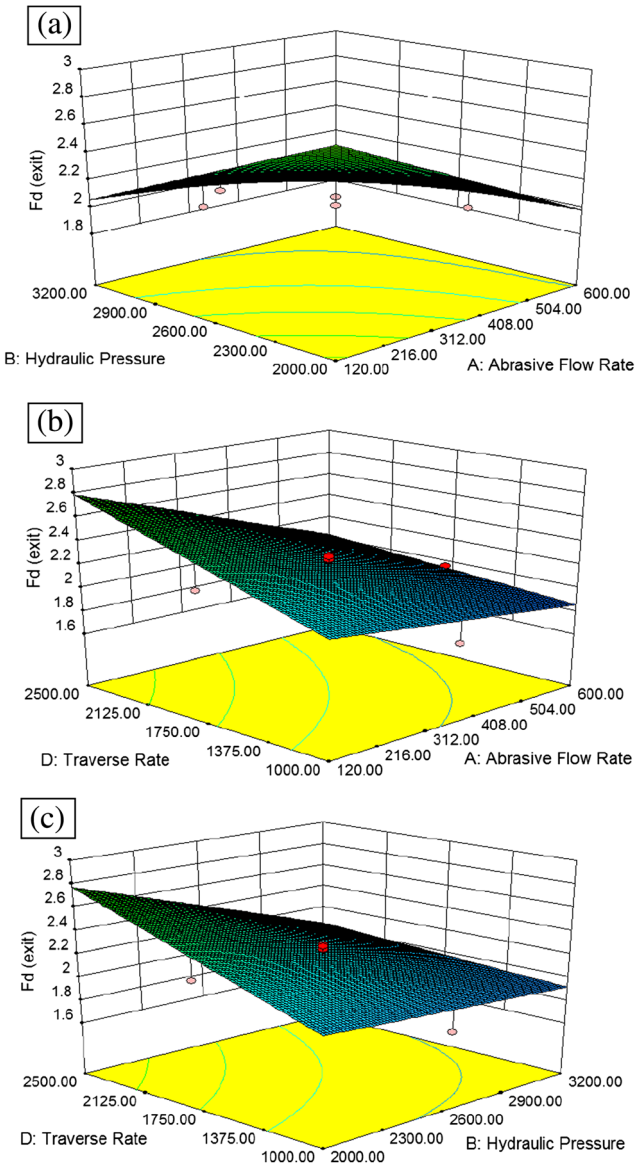

Fig. 15 Response surface and contour *plots*: interaction on $F_{d(\text{exit})}$ when the other variables are at middle level. **a** Abrasive flow rate and hydraulic pressure. **b** Abrasive flow rate and traverse rate. **c** Hydraulic pressure and traverse rate

3.3.5 Perturbation plot

Within the range of variables, a perturbation plot is shown in Fig. 16, which illustrated the effect of the AWJM process parameters on the delamination factor for the entrance and exit sides. This graph shows how the response changes as each variable moves from a chosen reference point when all other variables are held constant at a reference value. A curvature in the plot indicates that the response is sensitive to the factor. It is evident from Fig. 16a that both abrasive flow rate and hydraulic pressure have an adverse effect, whereas the traverse rate shows a positive effect on the delamination damage at the entrance side. As far as the stand-off distance is concerned, the result demonstrates that increasing the distance between the focusing nozzle and the workpiece until it reaches its centre value (5 mm) would result in severe delamination damage. Then, the delamination damage starts to drop as the stand-off distance increases above the centre line. Such behaviour could be attributed to the following reason as illustrated in Fig. 17. According to the impulse-change-momentum theorem [28], an object will experience the high impact of force if the change in momentum occurs over a short rate.

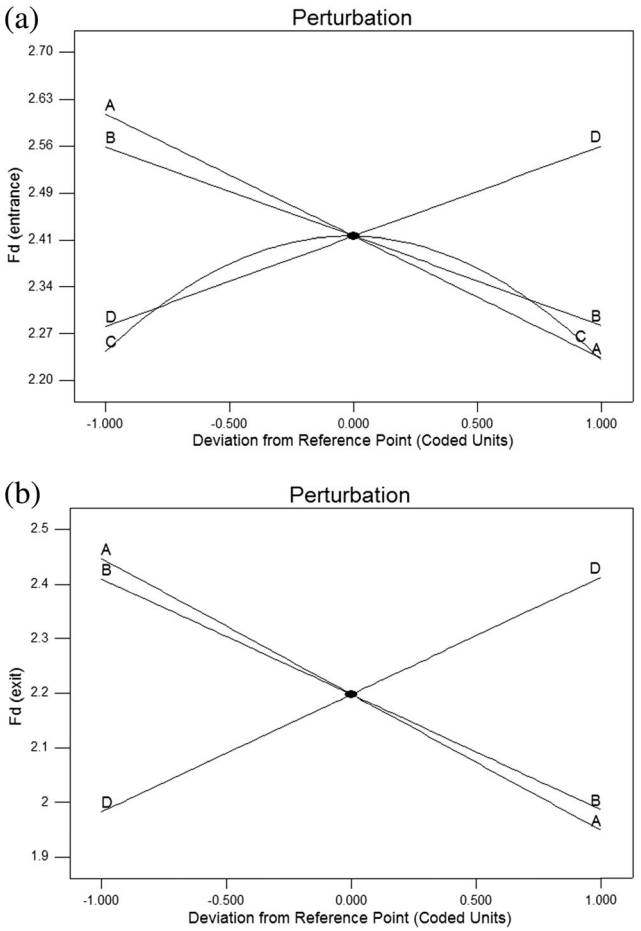

Fig. 16 *Perturbation plot* showing effect of all factors on **a** $F_{d(\text{entrance})}$ and **b** $F_{d(\text{exit})}$

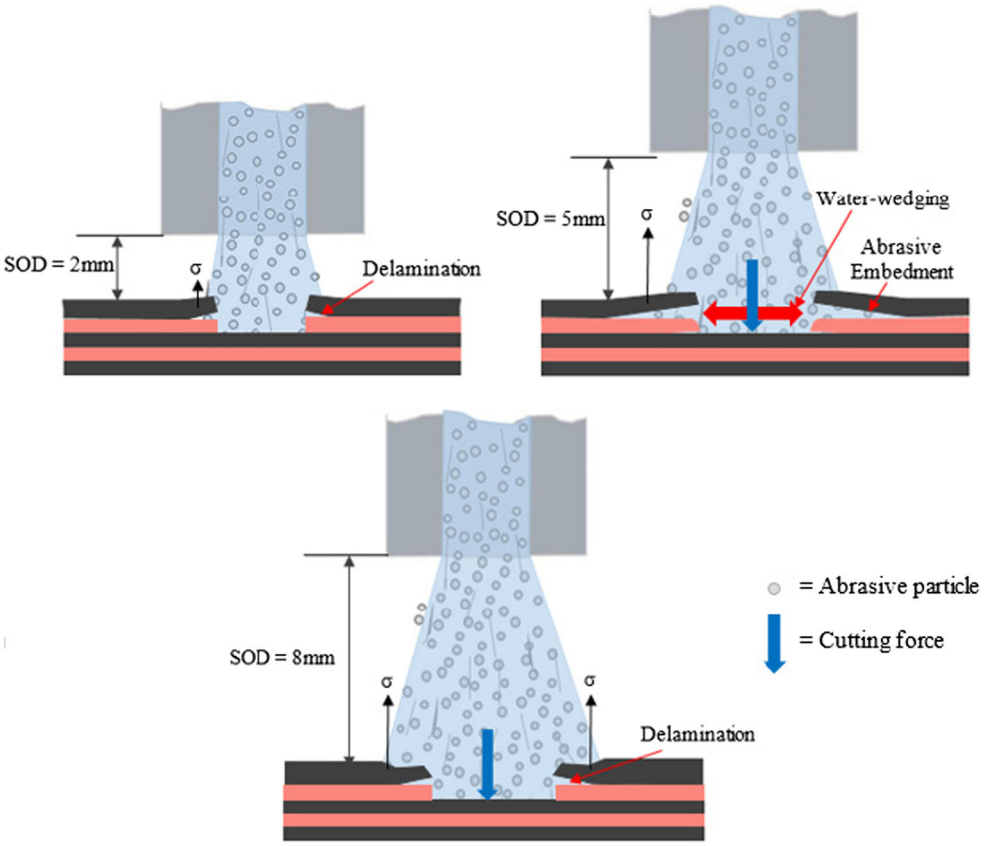

Fig. 17 Mechanism of delamination versus stand-off distance

Consequently, the momentum of the abrasive particle penetrated through composite laminates under a low stand-off distance will generate high impact force as well as collision force (Fig. 5.17a). This force allows the shearing of the fibre reinforcement rapidly as well as neat shaving and produces minimum interference with the internal laminate strength. Another essential point is that the high inter-collision of abrasive particles led by a united water-jet will produce a concentrated cutting force.

The increment in the stand-off distance will cause losses in the water-jet kinetic energy, and in the meantime, a diverging of the water-jet will appear. From Fig. 17b, it is clearly shown that the further enhancement of distance between nozzle and workpiece compared with Fig. 17a will create propagation of a crack tip. Apparently, delamination damage which occurred in the composite lamina is connected to the greater exerted impact force over the inter-lamina adhesive force that generates the crack tips. As the water flow continuously penetrates the composite, a water wedge action and embedment of the abrasive particle will be developed which enhances the delamination propagation [11]. Figure 17c demonstrates the larger expansion of the water-jet on the composite laminate with a 8-mm gap between nozzle and the workpiece set-up. Even though the results shown in Fig. 17a, c are similar, for effectiveness in the cutting process, a 2-mm-distance water-jet is preferable because the initially damaged region created on the entrance side is much lower compared to the 8-mm-distance water-jet.

From the aforementioned discussion, it can be observed that abrasive flow rate (A) is the most influential factor on

Table 14 Constraints for optimization of abrasive water-jet trimming process

Name	Goal	Lower limit	Upper limit	Importance
A: abrasive flow rate	Is in range	120	600	+++
B: hydraulic pressure	Is in range	200	320	+++
C: stand-off distance	Is in range	2	8	+++
D: traverse rate	Is in range	1000	2500	+++
T_R	Minimize	1.3000	1.9351	+++
F_d (entrance)	Minimize	1.7641	3.3207	+++
F_d (exit)	Minimize	1.6989	3.6005	+++

Table 15 Optimization results predicted using RSM methodology

No.	A	B	C	D	T_R	$F_{d(\text{entrance})}$	$F_{d(\text{exit})}$	Desirability	
1	600.00	2625.41	2.00	1000.00	1.31964	1.76413	1.86454	0.960	Selected
2	600.00	2601.32	2.00	1000.00	1.31963	1.76956	1.85993	0.960	
3	600.00	2632.48	2.00	1005.15	1.32012	1.76451	1.86645	0.959	
4	598.87	2578.60	2.00	1000.00	1.31962	1.77556	1.85619	0.959	
5	598.35	2565.52	2.00	1000.00	1.31963	1.77893	1.85399	0.959	

delamination on the entrance side followed by traverse rate (D) and hydraulic pressure (B). The change in abrasive flow rate and hydraulic pressure tends to increase the kinetic energy of the abrasive particle to trim the fibre reinforcement neatly, which minimizes the chances of the layers of plies to separate. On the other hand, under a slower traverse speed of the focusing nozzle, it increases the abrasive mass flow rate per unit area and decreases the penetration water-jet's trail back distance.

3.4 Optimization of trimming condition for hybrid FRP composites

Desirability function optimization of the RSM is a useful technique in analysing a system that comprises multi-response outputs. Very often, the multi-response output needs to be optimized simultaneously. In the optimization process, the kerf width is desired to be similar for the top width and the bottom width. This means that the ideal condition for the kerf ratio should be equal to 1. Meanwhile, delamination damage is the major component defect when machining a layered material. A high delamination damage value represents the critical delamination or cracks which are apparent at the interlaminate region. Therefore, the minimum value of F_d is desired or considered.

Table 14 shows the constraints and parameter ranges used during the optimization process, whereas Table 15 shows the optimization results for the process input parameters and its responses. Under the specified machining conditions, abrasive flow rate = 600 g/min, hydraulic pressure = 2626 MPa, stand-off distance =2 mm and traverse rate = 1000 mm/min are considered as the optimum trimming process parameters for AWJM which predicted a minimum value of T_R, F_d (entrance) and F_d (exit). Due to the restriction of the machine setting, the input parameter with decimal places is not valid. Therefore, the optimal parameters were rounded off. A validation experiment has been conducted according to the optimized setting, and the results are compared in Table 16, which depicted a range of 94–100% agreement with the predicted values.

4 Conclusions

This paper has discussed the trimming of hybrid carbon/glass fibre reinforcement polymer composites through abrasive water-jet machining (AWJM) process. Based on the experimental results and statistical analyses, stand-off distance was the dominating factor for minimization of the kerf ratio followed by traverse rate. The abrasive flow rate and hydraulic pressure showed insignificant influence on this response. The delamination damage of the hybrid composites was more severe on the entrance side as compared to the bottom side after cutting or erosion by the AWJM. The abrasive flow rate was the predominant factor for delamination damage followed by traverse rate and hybrid pressure. Minimum delamination damage can be achieved by increasing the kinetic energy of abrasive water-jet stream when impinging the composite under a lower speed. Meanwhile, an optimal set of process variables that yield the optimum quality features of the hybrid FRP composites produced by the AWJM process was also obtained. The optimum process parameters setting in achieving high-quality composites after the machining process were at abrasive flow rate of 600 g/min, hydraulic pressure of 2626 bar, stand-off distance of 2 mm and low traverse speed of 2500 mm/min. Finally, the confirmation test for the kerf ratio and delamination indicated that the prediction and regression model are within 5% of absolute error. Hence, the regression model is sufficient to predict the kerf ratio and delamination damage responses for AWJM of the hybrid FRP composites.

Table 16 Comparison of predicted value and actual validation run

	A	B	C	D	T_R	$F_{d(\text{entrance})}$	$F_{d(\text{exit})}$
Predicted	600.00	2625.41	2.00	1000.00	1.3196	1.7641	1.8646
Actual	600.00	2626.00	2.00	1000.00	1.3926	1.7630	1.9357
				Error (%):	5.2391	0.6409	3.6710

Acknowledgements The authors gratefully acknowledged the financial support of the Ministry of Science, Technology and Innovation (MOSTI) under the ScienceFund grant code UniMAP/RMIC/SF/06-01-15-SF0227/9005-00062. Technical supports from KTechno Sdn. Bhd. and Aerospace Composite Manufacturing Sdn. Bhd. are highly appreciated.

References

1. Dong C, Sudarisman, Davies IJ (2013) Flexural properties of E glass and TR50S carbon fiber reinforced epoxy hybrid composites. J Mater Eng Perform 22(1):41–49
2. Zhang J, Chaisombat K, He S, Wang CH (2012) Hybrid composite laminates reinforced with glass/carbon woven fabrics for lightweight load bearing structures. Mater Des 36:75–80
3. Kretsis G (1987) A review of the tensile compressive, flexural and shear properties of hybrid fiber-reinforced plastics. Compos 18(1): 13–23
4. Swolfs Y, Gorbatikh L, Verpoest I (2014) Fiber hybridisation in polymer composites: a review. Compos Part A 67(1):181–200
5. Haddad M, Zitoune R, Eyma F, Castanie B (2014) Study of the surface defects and dust generated during trimming of CFRP: influence of tool geometry, machining parameters and cutting speed range. Compos Part A 66:142–154
6. Sheikh-Ahmad J, Urban N, Cheraghi H (2012) Machining damage in edge trimming of CFRP. Mater Manuf Process 27:802–808
7. Tan CL, Azmi AI, Mohamad M (2014) Performance evaluations of carbon/glass hybrid polymer composites. Adv Mater Res 980:8–12
8. Hocheng H, Tsao CC (2003) Comprehensive analysis of delamination in drilling of composite materials with various drill bits. J Mater Process Technol 140:335–339
9. Azmi AI, Lin RJT, Bhattacharyya D (2013) Machinability study of glass fiber-reinforced polymer composites during end milling. Int J Adv Manuf Technol 64:247–261
10. Koplev A, Lystrup A (1983) The cutting process, chips and cutting forces in machining CFRP. Compos 14:371–376
11. Alberdi A, Suárez A, Artaza T, Escobar-Palafox GA, Ridgway K (2013) Composite cutting with abrasive water jet. Procedia Eng 63: 421–429
12. Ramulu M, Arola D (1994) The influence of abrasive waterjet cutting conditions on the surface quality of graphite/epoxy laminates. Int J Mach Tools Manuf 34(3):295–313
13. Ramulu M, Arola D (1993) Waterjet and abrasive waterjet cutting of unidirectional graphite epoxy composite. Compos 24:299–308
14. Azmir MA, Ahsan AK (2008) Investigation on glass/epoxy composite surfaces machined by abrasive water jet machining. J Mater Process Technol 198:122–128
15. Azmir MA, Ahsan AK (2009) A study of abrasive water jet machining process on glass/epoxy compsosite laminate. J Mater Process Technol 209:6168–6173
16. Shanmugam DK, Masood SH (2009) An investigation on kerf characteristics in abrasive waterjet cutting of layered composites. J Mater Process Technol 209:3887–3893
17. Shanmugam DK, Nguyen T, Wang J (2008) A study of delamination on graphite/epoxy composites in abrasive waterjet machining. Compos Part A 39:923–929
18. Zeng J, Olsen J, Olsen C. The abrasive waterjet as a precision metal cutting tool. 10th American Waterjet Conference. Houston, Texas. Paper 65
19. Irina MMW, Tan CL, Azmi AI, Leong KW, Mohd Radzi MN (2014) Evaluations of mechanical properties and residual strength of drilled glass fiber reinforced polymer (GFRP) composites. Appl Mech Mater 660:270–274
20. Irina MMW, Azmi AI, Tan CL, Lee CC, Khalil ANM (2015) Evaluation of mechanical properties of hybrid fiber reinforced polymer composites and their architecture. Procedia Manufac 2:236–240
21. Doreswamy D, Shivamurthy B, Anjaiah D, Sharma NY (2015) An investigation of abrasive water jet machining on graphite/glass/epoxy composite. Int J Manuf Eng 2015:1–11
22. Ambardekar VS, Shaikh AA (2013) An investigation on kerf geometry for abrasive waterjet cutting of metal-polymer-metal laminate. Int J Innov Technol Adapt Manag 1(2):1–5
23. Wang J (1999) A machinability study of polymer matrix composites using abrasive waterjet cutting technology. J Mater Process Technol 94:30–35
24. Unde PD, Gayakwad MD, Patil NG, Pawade RS, Thakur DG, Brahmankar PK (2015) Experimental investigations into abrasive waterjet machining of carbon fiber reinforced plastic. J Compos 2015:1–9
25. Ramulu M, Jenkins M, Guo Z (2001) Abrasive water jet machining mechanisms in continuous-fiber ceramic composites. J Compos Technol Res 23(2):82–91
26. Unde PD, Ghodke R (2015) Investigations of delamination in GFRP material cutting using abrasive waterjet machining. *Fourth Int. Conf. Adv. Mech. Aeronaut. Prod. Tech. – MAPT* 6–9
27. Abrate S, Walton D (1992) Machining of composite materials. Part II: Non-traditional methods Compos Manuf 3(2):8–94
28. Mott RL (2005) *Applied fluid mechanics*, Sixth Edit. University of Dayton: Pearson Education International